Part 4

Pulsar Wind Nebulae and Their Environments

https://doi.org/10.1017/S0074180900180830 Published online by Cambridge University Press

Young Neutron Stars and Their Environments
IAU Symposium, Vol. 218, 2004
F. Camilo and B. M. Gaensler, eds.

Theory of Pulsar Winds

A. Melatos
School of Physics, University of Melbourne, Parkville VIC 3010, Australia

Abstract. Recent progress in the theory of pulsar wind electrodynamics is reviewed, with emphasis on the following open questions. (i) Is the bipolar, jet-torus geometry imprinted by collimation or injection? (ii) what is the magnetic field geometry as a function of latitude, and is it stable? (iii) How rapidly does the postshock flow fluctuate, e.g. in the near infrared? (iv) The σ paradox: is Poynting flux converted gradually to kinetic energy flux as the wind expands, as in a linear accelerator, or is the conversion lossy, due to reconnection or parametric instabilities in a wave-like outflow?

1. Global Electrodynamics

A rotation-powered pulsar emits a relativistic (Lorentz factor $\gamma \gtrsim 10^5$) wind of leptons ($e^{\pm}$) generated in cascades in charge-starved regions of the magnetosphere. The injection rate is given by $\dot{N}_{\pm} = \kappa_{\pm}\dot{N}_{\rm GJ}$, where $e\dot{N}_{\rm GJ} = \Omega^2\mu/c$ is the Goldreich-Julian current, μ is the stellar magnetic moment, and the multiplicity satisfies $10 \lesssim \kappa_{\pm} \lesssim 10^3$ (Arons 2003). The wind may also contain dilute but energetic ions, with $\dot{N}_{\rm i} = \dot{N}_{\rm GJ}$ and $\dot{N}_{\rm i}\gamma m_{\rm i}c^2 \sim 0.5\dot{E}$, where $\dot{E} = I\Omega\dot{\Omega}$ is the spin-down luminosity. Magnetic flux is transported by the wind; the ratio, σ, of Poynting flux to kinetic energy flux is a key parameter. Although created hot ($k_{\rm B}T_{\pm} \sim \gamma m_{\rm e}c^2$) in pair cascades, the wind cools adiabatically ($T_{\pm} \propto r^{-1}$). Consequently, it does not shine and must be studied indirectly, via the radiation from the termination shock where it meets the environment — a supernova remnant, the interstellar medium, or material from a binary companion.

A recent advance in wind theory is the self-consistent solution for an aligned rotator constructed by Contopoulos et al. (1999). In this solution, which is force-free ($\rho\mathbf{E} + \mathbf{J} \times \mathbf{B}/c = 0$, where ρ and $\mathbf{J}$ denote the charge and current densities), magnetic flux surfaces, Ψ, are continuous at the light cylinder, $R_{\rm L} = c/\Omega$, where the Grad-Shafranov equation describing cross-field force balance has a regularizable singularity:

$$(1-x^2)\left(\frac{\partial^2\Psi}{\partial x^2} - \frac{1}{x}\frac{\partial\Psi}{\partial x} + \frac{\partial^2\Psi}{\partial z^2}\right) - 2x\frac{\partial\Psi}{\partial x} = -R_{\rm L}^2 A(\Psi)A'(\Psi)\ , \qquad (1)$$

with $\Psi_x(x=1) = AA'/2$. In Equation (1), (x,z) are cylindrical coordinates in a meridional plane, scaled to $R_{\rm L}$. Contopoulos et al. (1999) solved Equation (1) numerically by relaxation and found that the magnetosphere-plus-wind tends

toward a split monopole, $B_\phi = A(\Psi)/R \propto x^{-1}$ as $x \to \infty$, with a current $0.6e\dot{N}_{\rm GJ}$ flowing into the star ($0 \leq \Psi/\Psi_{\rm cap} \leq 1.08$, where $\Psi_{\rm cap}$ is the polar cap flux), and a return current $0.03e\dot{N}_{\rm GJ}$ flowing mainly along the open-closed separatrix and the equator ($1.08 \leq \Psi/\Psi_{\rm cap} \leq 1.36$). $\dot{E}$ is given by $1.36\Omega^4\mu^2/c^3$. The solution is uniquely specified up to the arbitrary location of the equatorial Y-point, here placed at $(x, z) = (1, 0)$, but it fails to converge reliably (Spitkovsky, these proceedings).

The wind of an oblique rotator is oscillatory; the conduction current ($nec \propto r^{-2}$) is insufficient to shield the displacement current ($\Omega E/4\pi \propto r^{-1}$) induced by the rotating star at distances $r \gtrsim 10^5 R_{\rm L}$ (Coroniti 1990; Melatos & Melrose 1996). It can take the form of an entropy wave, where stripes of alternating magnetic field separated by neutral sheets are convected with the flow (Coroniti 1990; Lyubarsky & Kirk 2001), or a sub/superluminal relativistic plasma wave (Melatos & Melrose 1996; Melatos 1998; Arons 2003). The polarization is circular along the rotation axis, where the optical and X-ray jets and knots are observed in pulsar wind nebulae (PWNe), and linear in the equatorial plane, where the wisps and torus are located (Hester et al. 2002; Gaensler et al. 2002). The wave is globally coherent and of large amplitude ($a = eE/m_{\rm e}c\Omega \gg 1$).

Bogovalov (1999) showed that, under ideal-magnetohydrodynamic (MHD) conditions, the magnetosphere and wind of an oblique rotator can be constructed directly from the aligned rotator solution. The result is an oscillatory split monopole with a corrugated equatorial current sheet, viz. $B_r = B_0 R_{\rm L}^2 r^{-2} f(r,t)$, $B_\phi = E_\theta = -B_0 R_{\rm L} r^{-1} \sin\theta f(r,t)$, $B_0 = 1.36\mu R_{\rm L}^{-3}$, and $f(r,t) = {\rm sgn}[{\rm mod}(r/R_{\rm L}, 2\pi) - \phi + \Omega t]$. However, this solution is unphysical for three reasons. (i) It requires the fluid density and velocity to satisfy $\partial/\partial t = \partial/\partial\phi = 0$ everywhere, yet this condition is clearly violated near $R_{\rm L}$ because the magnetosphere is not axisymmetric. That is, the solution is inconsistent with the oscillatory inner boundary condition at $R_{\rm L}$, which drives a wave in the *particles* as well as the fields. (ii) Self-consistent relativistic plasma wave solutions for the displacement-current-dominated outer wind ($r \gtrsim 10^5 R_{\rm L}$) do not obey ideal MHD, nor do the associated fluid density and velocity satisfy $\partial/\partial t = \partial/\partial\phi = 0$ (Melatos & Melrose 1996). (iii) The region $r \gtrsim 10^5 R_{\rm L}$ acts approximately as an electrodynamic vacuum ($nec \ll \Omega E/4\pi$), so one expects outgoing magnetic *dipole* radiation as $r \to \infty$ (energy flux $\propto 1 + \cos^2\theta$), even if the antenna is a split monopole.

I take this opportunity to clarify a common misconception concerning the pulsar braking index n for spin down via a wind. One has $n = 3$, as for the vacuum dipole, as long as the wind is Poynting-dominated at $R_{\rm L}$. One does not have $n = 1$, as suggested sometimes, unless the radiation fields are monopolar (which is unphysical) or the wind is kinetic-dominated at $R_{\rm L}$, in which case $n \neq 3$ in general but $n = 1$ is just one possibility among many.

2. Collimation and Cylindrical Symmetry

Multiwavelength imaging of PWNe at subarcsecond resolution reveals a characteristic, crossbow-like morphology, symmetric about the pulsar's rotation axis. Arc-like features (optical wisps, X-ray torus) and axial features (optical knots, X-ray jet) coexist and are identified with the termination shock at equatorial

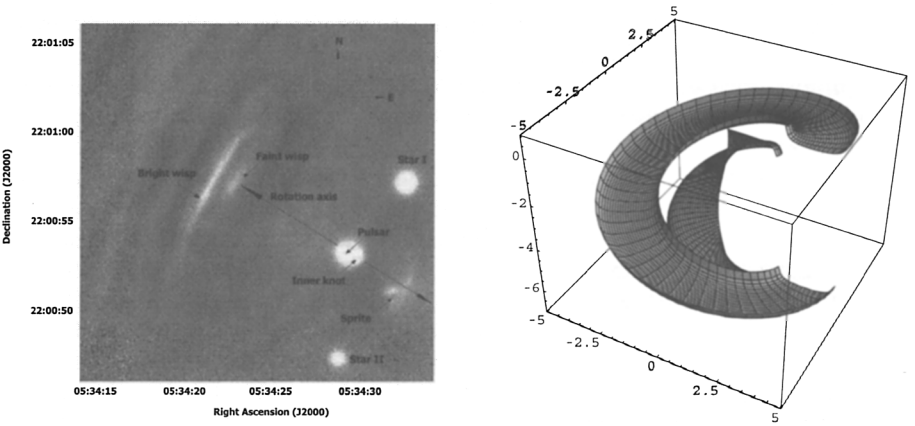

Figure 1. (a) Near-infrared, adaptive optics image of the inner $20'' \times 20''$ of the Crab nebula. (b) Force-free final state of the MHD kink instability in a conducting cylinder; the surface is $B_\phi = \text{constant}$.

and polar latitudes respectively. Examples include the Crab (Hester et al. 1995, 2002), Vela (Pavlov et al. 2003), and G320.4–1.2 (Gaensler et al. 2002). The crossbow morphology is apparent in Figure 1(a), corresponding] to an image of the Crab in K' taken with the Hokupa'a/QUIRC adaptive optics camera on the Gemini North Telescope (Melatos et al. 2004). All features are variable on time-scales shorter than one day, as described in §4.

Two mechanisms can collimate the wind *upstream* from the termination shock, at least in principle. (i) MHD hoop stress ($\mathbf{J} \times \mathbf{B}$) causes magnetic flux surfaces to converge to nested paraboloids or cylinders as $r \to \infty$ (Begelman & Li 1994). However, this occurs too gradually ($\propto \log r$), because the electric force nearly balances the hoop stress in a relativistic flow, with $\rho\mathbf{E} + \mathbf{J} \times \mathbf{B} \approx 0$. (ii) The ponderomotive force in a wave-like wind may focus the plasma toward the poles (see §1 and Arons 2003). However, the ponderomotive force is nearly radial ($\propto \nabla E^2$), with a θ component $r/r_{\rm L}$ times smaller, so the effect is weak. (The radial force accelerates $e^{\pm}$ to $\gamma \sim a^2$.)

Several mechanisms can cause *downstream* collimation. (iii) MHD hoop stress is effective (Okamoto 2000), because the flow is nonrelativistic, with $\rho\mathbf{E} \ll \mathbf{J} \times \mathbf{B}$. (iv) If the energy flux in the wind decreases toward the poles, external pressure confinement tends to produce a jet (Lyubarsky & Eichler 2001). The wind may also interact with a cylindrically symmetric presupernova wind cavity, although there is no reason why the symmetry axis should coincide with the postsupernova rotation axis of the pulsar (Pavlov et al. 2003). (v) The postshock magnetic field may evolve toward a helical, bipolar geometry through the MHD kink instability (Begelman 1998; Melatos 2004).

Mechanism (iv) was investigated by Komissarov & Lyubarsky (2003). Starting with the energy flux of a split monopole $\propto \sin^2\theta$, a toroidal magnetic field $\langle B_\phi \rangle \propto (1 - 2\theta/\pi)\sin\theta$, and synchrotron $e^{\pm}$ with an $\varepsilon^{-2.2}$ energy spectrum, they explained the wisps as a network of intersecting shocks in the backflow from the supernova remnant, viewed in projection and subjected to Doppler

https://doi.org/10.1017/S0074180900180830 Published online by Cambridge University Press

boosting. The jet is launched by the heightened pressure where the hoop stress decelerates the surface layers of the equatorial outflow; no jet forms for $\sigma < 0.04$. The model does not specify the particle flux as a function of latitude, but the implied uncertainty in the synchrotron emissivity is small (Lyubarsky, private communication).

Mechanism (v) was investigated by Begelman (1998), who showed that the ordered B_ϕ in the Crab is unstable to MHD kink modes at $r \approx 3r_s$, where r_s is the distance to the termination shock. He surmised that the instability evolves nonlinearly to break up B_ϕ into small magnetic loops (and, incidentally, alleviate the σ paradox; see §3). However, laboratory experiments (e.g. reverse-field pinches) prove that the kink instability can evolve to other states too; for example, an ordered B_ϕ may be regenerated by a mean-field α dynamo (sawtooth oscillations), at least in a configuration confined by conducting walls (e.g. the supernova remnant; Biskamp 1993; Melatos 2004). The final state minimizes magnetic energy while conserving helicity and is therefore force-free ($\nabla \times \mathbf{B} = k\mathbf{B}$). It adopts a helical geometry as in Figure 1(b) for $k > 39/r_s c^2$, where k parametrizes the axial current in the nebula (Melatos 2004).

3. Energy Transport

The ratio of Poynting flux to kinetic energy flux, $\sigma = B_\phi^2/8\pi n_\pm \gamma m_e c^2$, where $n_\pm$ denotes the pair number density, is a key parameter in pulsar wind theories. Models of magnetospheric pair cascades (Arons 2003) imply $\sigma(r_L) = e\Phi_{cap}/2\gamma m_{eff} c^2 \gg 1$, with $m_{eff} = m_i + 2\kappa_\pm m_e$ and $\Phi = \Omega^2\mu/c^2$ (open field line voltage). On the other hand, observations of the termination shock imply $10^{-2} \lesssim \sigma(r_s) \lesssim 10^{-3}$ in both the Crab and PSR B1509–58 (Kennel & Coroniti 1984; Gaensler et al. 2002); the hoop stress must be weak to allow the flow to decelerate from $c/3$ at r_s to $\sim 10^3$ km s^{-1} at the supernova remnant.

The twin constraints $\sigma(r_L) \gg 1$ and $\sigma(r_s) \ll 1$ are inconsistent with steady-state, ideal-MHD wind theories. Naively, one expects $B_\phi \propto r^{-1}$, $n_\pm \propto r^{-2}$, and $\gamma =$ constant in such a theory, implying that σ is independent of r: the σ paradox. Recent work has led to a more sophisticated understanding of this issue, without altering the basic conclusion. Contopoulos & Kazanas (2002) showed that a linear accelerator operates in the split-monopole geometry of a force-free aligned rotator, with $\gamma = (1 + x^2)^{1/2}$ and hence $\sigma \propto x^{-1}$. The acceleration is due to a (slight) increase with r in the MHD drift velocity $\mathbf{v}_E = c\mathbf{E} \times \mathbf{B}/B^2$, or, equivalently, to the work done by $\mathbf{E}$ in the presence of the (small) inertial drift $\mathbf{v}_d = (m_e c/eB^2)\mathbf{B} \times d(\gamma \mathbf{v}_E)/dt$ (Arons 2003). However, the linear accelerator shuts off in the region $r \gtrsim [\sigma(R_L)]^{1/3} R_L \ll r_s$, where the wind speed exceeds the local magnetosonic speed and magnetic stresses are not communicated back to the star. Consequently, one finds $\sigma(r_s) \approx [\sigma(R_L)]^{2/3} \gg 1$, contrary to observations (Arons, these proceedings).

Is the high-to-low-σ transition lossy or lossless? A dissipative transition ought to produce intense high-energy radiation (luminosity $\sim \dot{E}$) from the wind zone, yet this is not observed. Indeed, the only wind emission detected to date is the axial inner knot in the Crab and PSR B1509–58, at $r \approx 10^{-2} r_s$, with optical luminosity $\sim 10^{-6}\dot{E}$ (Hester et al. 1995, 2002; Gaensler et al. 2002). Relativistic beaming offers a loophole, provided that the dissipation is equatorial

(i.e. $|\theta - \pi/2| \lesssim 10°$). In one appealing mechanism of this sort, the alternating B_ϕ in the entropy mode is annihilated by magnetic reconnection (Coroniti 1990; Lyubarsky & Kirk 2001). Unfortunately, reconnection-driven heating also accelerates the flow, dilating the reconnection rate in the observer's frame, so that σ is reduced too gradually to explain $\sigma(r_s) \approx 10^{-3}$ (Lyubarsky & Kirk 2001), unless reconnection occurs in the shock itself (Lyubarsky 2003). It will be valuable to incorporate the results of modern laboratory experiments (e.g. MRX; Ji et al. 1998) into the above models, as these experiments lead to a new picture of reconnection physics in which the rate takes the Sweet-Parker value, $(4\pi\lambda V_A/\eta c^2)^{-1/2}$, and the anomalous resistivity is due to whistler and lower-hybrid waves generated by the electron inertia and Hall effects. (Here, λ, V_A, and η denote respectively the neutral sheet width, Alfvén speed, and anomalous resistivity corrected for compressibility and downstream pressure).

A dissipationless transition from high to low σ can occur in a wave-like, displacement-current-dominated wind. Melatos & Melrose (1996) showed that such a wind is *necessarily* kinetic-dominated in the region $r \gtrsim 10^5 r_L$, with $\sigma(r_s) \approx m_e c^3 r^2/\dot{N}_\pm \gamma e^2 R_L^2$ for the circularly polarized, superluminal mode propagating at polar latitudes. Indeed, for $\dot{N}_\pm = 10^{38}\,s^{-1}$ and $\gamma = 10^6$ (Gallant & Arons 1994), one finds $\sigma \approx 4 \times 10^{-3}$, as observed. Physically, this is because the ponderomotive force of the wave accelerates $e^\pm$ efficiently (see §2); the bulk frame electric field is large. If a nonzero radial magnetic field is included, with $B_r \propto r^{-2}$ as for the aligned rotator, two circularly polarized modes exist: the superluminal mode above, and a subluminal mode that is analogous to an inertial Alfvén wave (Melatos 1998). Figure 2(a) illustrates how energy is transported by the modes. Near r_L, only the subluminal, high-σ mode can propagate; near r_s, only the superluminal, low-σ mode can propagate; and in the region $10^6 \lesssim r/r_L \lesssim 10^7$, energy passes from the subluminal to the superluminal mode as the latter is disrupted by magneto-parametric instabilities (Melatos 1998). This mechanism faces two difficulties: (i) it is hard to understand why it would be radiatively silent, given the randomization of particle motions as the wave is disrupted nonlinearly; and (ii) it does not apply straightforwardly to the equatorial plane, where the wave is linearly polarized and the Poynting and kinetic energy fluxes both depend on a. Melatos (1998) postulated that the inner knot in the Crab represents synchro-Compton radiation from the region $10^6 \lesssim r/r_L \lesssim 10^7$ and is therefore a signature of an instability-driven σ transition. Polarization data can test this hypothesis.

Begelman (1998) claimed that the σ paradox is resolved if the MHD kink instability disrupts B_ϕ into small magnetic loops, because then the mean hoop stress is zero and the condition $\sigma(r_s) \ll 1$ is unnecessary for matching the expansion speed of the nebula. However, even if the ordered B_ϕ is zero, the isotropic magnetic pressure exerted by the loops (which mimic a $\Gamma = 4/3$ gas) prevents a high-σ flow from decelerating, provided that the loops press against an external wall (e.g. the supernova remnant) when compressed. Moreover, in the presence of a conducting wall, the kink-unstable magnetic field can evolve nonlinearly to an ordered cylindrical or helical structure (instead of loops), for which the hoop stress is large, as shown in §2 and Figure 1(b).

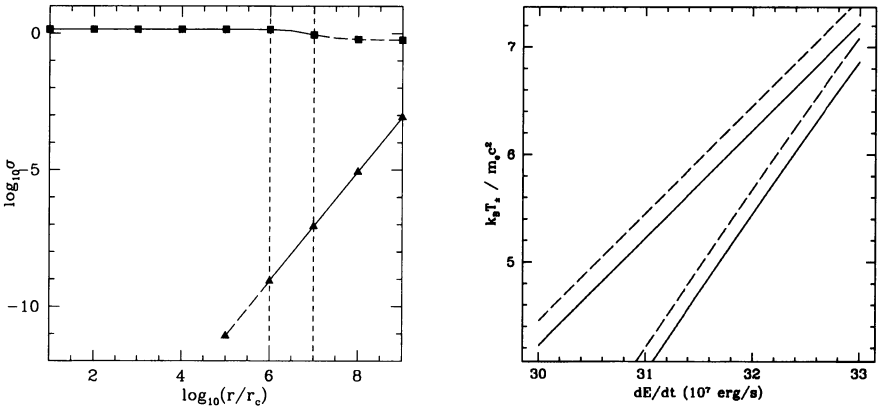

Figure 2. (a) Ratio of Poynting flux to kinetic energy flux, σ, versus radial distance, r, for the subluminal (top) and superluminal (bottom) modes. Solid (dashed) regions are stable (unstable) respectively. (b) Downstream pair temperature, $k_{\rm B}T_{\pm}/m_{\rm e}c^2$, versus spin-down luminosity, $\dot{E}$ (watts), for a wave-like shock with $\sigma = 10^{-3}$, 10^{0} (top, bottom) and $V = 0.84c$, $0.36c$ (solid, dashed) (Finn, private communication).

4. Variability of the Termination Shock

Multiwavelength imaging of PWNe reveals that the equatorial and polar structures described in §2 vary daily. In the Crab, the wisps propagate away from the pulsar as circular ripples (pattern speed $\approx 0.5c$), with randomly fluctuating fibrous substructure, while the polar knots change position and brightness quasiperiodically, with blobs emerging from the working surface of the jet and propagating outward at $\approx 0.4c$ (Hester et al. 2002). In Vela, the knotty jet changes its shape and spectrum weekly and daily respectively (Pavlov et al. 2003).

Spitkovsky & Arons (2004) explained the wisp variability in terms of ion cyclotron acceleration at the termination shock. Cold upstream ions gyrate forward ($\mathbf{E}\times\mathbf{B}$ drift) at the magnetic step of the shock, compressing the frozen-in magnetic field into spikes which react back to marshal the ions cyclically into bunches (i.e. wisps) which propagate downstream before thermalizing over several Larmor radii by absorbing ion-powered magnetosonic waves (Gallant & Arons 1994; Spitkovsky & Arons 2004). The theory correctly predicts the wisp luminosity (including Doppler boosting), spacing, variability, and pattern speed for $\dot{N}_{\rm i} = \dot{N}_{\rm GJ}$, $\gamma = 4\times10^5$, $\kappa_{\pm} = 10^3$, and $\dot{N}_{\rm i}\gamma m_{\rm i}c^2 \approx 0.2\dot{E}$ for the Crab, and similar parameters for PSR B1509–58 (Gaensler et al. 2002; Spitkovsky & Arons 2004). The variability time-scale is roughly half the ion cyclotron period (≈ 6 months) in the downstream magnetic field, $B_s \approx 0.3\,$mG.

An alternative model for the jet-torus morphology of PWNe is based on intersecting internal shocks (see §2; Komissarov & Lyubarsky 2003). As published, the model is steady-state, but it can support variability, e.g. due to Kelvin-Helmholtz instabilities in the shear layer between the equatorial outflow

https://doi.org/10.1017/S0074180900180830 Published online by Cambridge University Press

and backflow, or a synchrotron cooling instability (Hester et al. 2002). It will be interesting to verify whether such processes operate quasiperiodically, as observed for the wisps, and on the correct time-scale.

The variability of the Crab wisps and knots appears to extend to time-scales as short as 10 min. Near-infrared (J and K') imaging with the Hokupa'a/QUIRC adaptive optics camera on the Gemini North Telescope reveals surface brightness fluctuations between 10% and 30% in J (Melatos et al. 2004), although photometry is impaired by the unsteady nebula background and adaptive-optics PSF. Variability on this time-scale is surprising, although the flow is Doppler boosted. One possible mechanism is the relativistic fire hose instability, driven by anisotropy of the kinetic pressure $\langle v_i v_j \rangle$ parallel and perpendicular to the magnetic field, which grows on the $e^{\pm}$ cyclotron period $\approx 0.14 m_e \langle \gamma \rangle / eB \approx 1$ hr (Pavlov et al. 2003; Melatos et al. 2004). Equally surprisingly, the near-infrared flux densities of the inner knot and wisps scale as $\nu^{-0.7}$, compared to $\nu^{-0.2}$ for the sprite (Melatos et al. 2004) — yet the sprite and wisps are produced by similar physics (synchrotron emission from the termination shock) whereas the inner knot resides in the unshocked wind and is probably the result of another process (e.g. synchro-Compton emission from a relativistic plasma wave).

How is the shock physics altered if the wind is wave-like? In a striped wind (entropy mode), a standard MHD shock is maintained (Kennel & Coroniti 1984), except that the alternating B_ϕ reconnects as the flow decelerates. The Rankine-Hugoniot jump conditions are functions of a single parameter, $\chi = f\sigma(1+\sigma)^{-1}$, where $1-f$ measures the annihilated fraction of the magnetic energy; for example, the downstream flow speed is $V \approx c(1+4\chi)/3$ for $\chi \ll 1$ (Lyubarsky 2003). Numerical simulations are needed to verify how reconnection occurs; tearing modes are one possibility, but the physics is modified because the wavelength of $e^{\pm}$ trajectories in the wave ($\sim aR_{\rm L}$) is much smaller than the $e^{\pm}$ Larmor radius. For a transverse, circularly polarized, subluminal or superluminal mode, Mastrano et al. (2004) found that two downstream flow solutions exist, with $V = 0.84c$ and $V = 0.36c$, assuming that the wave frequency Ω does not change across the step. Figure 2(b) plots the downstream pair temperature $T_\pm$ as a function of $\dot{E}$ for $\sigma \ll 1$ and $\sigma \gg 1$. Numerical simulations are needed to determine if the system tends to the fast or slow solution, and to check whether the downstream wave is stable; parametric instabilities grow on a time-scale $\sim \Omega^{-1}$ in a nonrelativistic bulk flow but can be suppressed thermally.

5. Future Directions

Although a theory of pulsar wind electrodynamics has proved elusive, there are reasons to be optimistic in light of recent progress. Spitkovsky (these proceedings) has proved that it is (nearly) possible to simulate the magnetosphere of an oblique rotator numerically. His simulations produce a dome-disk electrosphere that flops due to the diocotron instability. Near $R_{\rm L}$, the momentum in the electromagnetic wave fields is imparted to the charges, driving off what appears to be the beginning of a spiral wind. The next task is to match this inner boundary condition to an outgoing relativistic plasma wave, in order to calculate the particle flux, energy flux, and magnetic field as a function of latitude. In my opinion, this needs to be approached from a two-fluid viewpoint (to avoid the ideal-MHD approximation, which ignores large terms like the electron inertia in

https://doi.org/10.1017/S0074180900180830 Published online by Cambridge University Press

the generalized Ohm's law; cf. Lyubarsky 2003) and as an antenna problem *in medio* (to drive a wave in the particles as well as the fields at the nonaxisymmetric inner boundary; cf. Bogovalov 1999). Nevertheless, preliminary progress on wave solutions has been made — enough to demonstrate unequivocally that energy transport in a wave-like wind differs from the steady state (e.g. Melatos 1998; Lyubarsky & Kirk 2001). The revival of the linear accelerator in the split-monopole wind of an aligned rotator, although unable to resolve the σ paradox (Contopoulos & Kazanas 2002; Arons 2003 and these proceedings), remains a key input into future wave theories, where it is often postulated that the wind resembles the aligned rotator when averaged over the fast oscillation, Ω. Once a basic wave solution $\propto \exp(i\Omega t)$ is found, it will be interesting to investigate its disruption by parametric instabilities and wave breaking, and its interaction with the corrugated equatorial current sheet, in order to probe the transition from a high-σ to a low-σ flow.

References

Arons, J. 2003, ApJ, 589, 871
Begelman, M. C. 1998, ApJ, 493, 291
Begelman, M. C., Li, Z.-Y. 1994, ApJ, 426, 269
Biskamp, D. 1993, Nonlinear Magnetohydrodynamics, (Cambridge: CUP)
Bogovalov, S. V. 1999, A&A, 349, 1017
Contopoulos, I., & Kazanas, D. 2002, ApJ, 566, 336
Contopoulos, I., Kazanas, D., & Fendt, C. 1999, ApJ, 511, 351
Coroniti, F. V. 1990, ApJ, 349, 538
Gaensler, B. M. et al. 2002, ApJ, 569, 878
Gallant, Y. A., & Arons, J. 1994, ApJ, 435, 230
Hester, J. J. et al. 1995, ApJ, 448, 240
Hester, J. J. et al. 2002, ApJ, 577, L49
Ji, H., Yamada, M., Hsu, S., & Kulsrud, R. 1998, Phys. Rev. Lett., 80, 3256
Kennel, C. F., & Coroniti, F. V. 1984, ApJ, 283, 694
Komissarov, S. S., & Lyubarsky, Y. E. 2003, MNRAS, 344, L93
Lyubarsky, Y. 2003, MNRAS, 345, 153
Lyubarsky, Y., & Eichler, D. 2001, ApJ, 562, 494
Lyubarsky, Y., & Kirk, J. 2001, ApJ, 547, 437
Mastrano, A., Melatos, A., & Finn, C. R. 2004, MNRAS, in preparation
Melatos, A. 1998, Mem. Soc. Ast. It., 69, 1009
— 2004, ApJ, submitted
Melatos, A., & Melrose, D. B. 1996, MNRAS, 279, 1168
Melatos, A. et al. 2004, ApJ, submitted
Okamoto, I. 2000, MNRAS, 318, 250
Pavlov, G. G. et al. 2003, ApJ, 591, 1157
Spitkovsky, A., & Arons, J. 2004, ApJ, 603, 669